Redox Biology 72 (2024) 103159

Contents lists available at ScienceDirect

Redox Biology

journal homepage: www.elsevier.com/locate/redox

SLC7A11-ROS/αKG-AMPK axis regulates liver inflammation through mitophagy and impairs liver fibrosis and NASH progression

Tingting Lv [a,b,c,1], Xiude Fan [d,1], Chang He [e,1], Suwei Zhu [f], Xiaofeng Xiong [g], Wei Yan [g], Mei Liu [g], Hongwei Xu [a,**], Ruihua Shi [c,***], Qin He [a,c,*]

[a] Department of Gastroenterology, Shandong Provincial Hospital Affiliated to Shandong First Medical University, Jinan, Shandong, 250021, China
[b] Department of Cancer Center, Shandong Provincial Hospital Affiliated to Shandong First Medical University, Jinan, Shandong, 250021, China
[c] Department of Gastroenterology, Zhongda Hospital Affiliated to Southeast University, Nanjing, Jiangsu, 210009, China
[d] Key Laboratory of Endocrine Glucose & Lipids Metabolism and Brain Aging, Ministry of Education, Department of Endocrinology, Shandong Provincial Hospital Affiliated to Shandong First Medical University, Jinan, Shandong, 250021, China
[e] Medical College, Nantong University, Nantong, Jiangsu, 226001, China
[f] Department of Critical Care Medicine, Shandong Provincial Hospital Affiliated to Shandong First Medical University, Jinan, Shandong, 250021, China
[g] Department of Gastroenterology, Institute of Liver and Gastrointestinal Diseases, Tongji Hospital of Tongji Medical College, Huazhong University of Science and Technology, Wuhan, Hubei, 430030, China

ARTICLE INFO

Keywords:
Nonalcoholic steatohepatitis
SLC7A11
AMPK
NLRP3 inflammasome
Mitophagy

ABSTRACT

The changes of inflammation and metabolism are two features in nonalcoholic steatohepatitis (NASH). However, how they interact to regulate NASH progression remains largely unknown. Our works have demonstrated the importance of solute carrier family 7 member 11 (SLC7A11) in inflammation and metabolism. Nevertheless, whether SLC7A11 regulates NASH progression through mediating inflammation and metabolism is unclear. In this study, we found that SLC7A11 expression was increased in liver samples from patients with NASH. Upregulated SLC7A11 level was also detected in two murine NASH models. Functional studies showed that SLC7A11 knockdown or knockout had augmented steatohepatitis with suppression of inflammatory markers in mice. However, overexpression of SLC7A11 dramatically alleviated diet-induced NASH pathogenesis. Mechanically, SLC7A11 decreased reactive oxygen species (ROS) level and promoted α-ketoglutarate (αKG)/prolyl hydroxylase (PHD) activity, which activated AMPK pathway. Furthermore, SLC7A11 impaired expression of NLRP3 inflammasome components through AMPK-mitophagy axis. IL-1β release through NLRP3 inflammasome recruited myeloid cells and promoted hepatic stellate cells (HSCs) activation, which contributed to the progression of liver injury and fibrosis. Anti-IL-1β and anakinra might attenuate the hepatic inflammatory response evoked by SLC7A11 knockdown. Moreover, the upregulation of SLC7A11 in NASH was contributed by lipid overload-induced JNK-c-Jun pathway. In conclusions, SLC7A11 acts as a protective factor in controlling the development of NASH. Upregulation of SLC7A11 is protective by regulating oxidation, αKG and energy metabolism, decreasing inflammation and fibrosis.

1. Introduction

Nonalcoholic fatty liver disease (NAFLD) is one of the most prevalent chronic liver diseases, affecting approximately one quarter of the global population worldwide. Nonalcoholic steatohepatitis (NASH) is a progressive type of NAFLD and is associated with inflammation and fibrosis, which may progress to cirrhosis and hepatocellular carcinoma (HCC) [1–3]. Although our understanding of NAFLD-NASH pathophysiology continues to advance rapidly, there are currently no approved therapies [4,5]. As a metabolic and inflammatory disease, how

* Corresponding author. Department of Gastroenterology, Shandong Provincial Hospital Affiliated to Shandong First Medical University, Jinan, Shandong, 250021, China.
** Corresponding author.
*** Corresponding author.
E-mail addresses: xhwsdslyy@sina.com (H. Xu), ruihuashi@126.com (R. Shi), heqin@sdfmu.edu.cn (Q. He).
[1] These authors contributed equally to this work.

https://doi.org/10.1016/j.redox.2024.103159
Received 25 March 2024; Received in revised form 10 April 2024; Accepted 13 April 2024
Available online 16 April 2024

metabolic disorder transits to uncontrollable inflammation remains unclear.

Lipometabolic disturbance in liver causes lipotoxicity, which leads to reactive oxygen species (ROS) accumulation [6,7]. ROS with high concentrations in cells causes macromolecules damage by oxidative modifications in cellular macromolecules and leads to cell damage, inflammation and fibrosis [8–10]. In early stages of NAFLD, mitochondrial respiratory functions are increased to mitigate disease progression. Yet in NASH, mitochondrial adaptations are completely lost, and a low respiration rate and increased mitochondrial mass were observed [11,12]. Therefore, mitochondrial metabolism functions a vital role in NASH progression. Even though, the regulation of oxidative and mitochondrial metabolism, and their effects in mediating the crosstalk between hepatocytes and HSCs during fibrosis development in NASH remains largely unknown.

As a member of the SLC7 family of amino acid transporters, solute carrier family 7 member 11 (SLC7A11) is responsible for importing cysteine and outputting glutamate, a rate-limiting precursor for synthesis of the antioxidant glutathione (GSH) [13,14]. SLC7A11 is vital for decreased ROS level and elevated α-ketoglutarate (αKG) content [15]. Oxidative metabolism acts as a trigger for immune responses, inflammation and progression of NASH [16,17]. Our previous study has also demonstrated that SLC7A11-induced decrease of αKG involves in inflammation [15]. Therefore, we hypothesized that SLC7A11 could act in the progression of NASH.

In this study, we documented that increased SLC7A11 might serve as a protective role with upregulated expression in NASH samples, and connected with severity of the disease. SLC7A11 knockdown or knockout in mice had advanced lesion in NASH. However, overexpression of SLC7A11 had the protective effect. Mechanically, SLC7A11 decreased ROS level and αKG content by exchanging cysteine and glutamate, which activated adenosine monophosphate (AMP)–activated protein kinase (AMPK) pathway. The AMPK pathway decreased expression of NLRP3 inflammasome components by promoting mitophagy. IL-1β from NLRP3 inflammasome recruited myeloid cells and activated HSCs, which promoted liver fibrosis in SLC7A11 knockdown mice. Finally, we found that lipid-induced JNK pathway contributed to the upregulation of SLC7A11 by c-Jun. These works indicate that SLC7A11 is a critical regulator in the development of NASH.

2. Materials and methods

2.1. Human liver samples

Human liver samples were obtained from patients undergoing liver biopsy, liver surgery or liver transplantation. The exclusion criteria were described as following: individuals with a history of excessive alcohol consumption (>140 g for men or >70 g for women, per week), drug or toxin use, viral infection or other liver diseases were excluded from the study [18,19]. The study was approved by the institutional ethics committee of Shandong provincial hospital and adhered to the principles of the Declaration of Helsinki. NAFLD activity score (NAS) was following the roles: cases with a NAS ≥3 or 5 were classified as NAFLD and NASH respectively. Samples with NAS of 0 were treated as normal controls (NC) [20].

2.2. Animal studies

All animal protocols were approved by the Institutional Animal Care and Use Committee of Shandong provincial hospital. SLC7A11 knockout mice were obtained from Cyagen Biosciences. Hepatic knockdown or overexpression of SLC7A11 was applied by adeno-associated virus (AAV). All mice (C57BL/6 male) were housed in temperature-controlled environment (23 ± 2 °C) with a 12 h/12 h light/dark cycle. Mice were fed either normal chow (NC) or high-fat/high-cholesterol (HFHC) for 28 weeks [21] or methionine-choline deficient (MCD) diet for 8 weeks [22], which caused NASH. Compound C (25 mg/kg; i.p. daily for one week) was used to inhibit AMPK in mice [23]. In the DM-αKG treatment, mice also received control vehicle or DM-αKG (0.6 g per kg body weight) [24]. Anakinra was administered daily (1 mg/kg i.p.). Neutralizing Abs against IL-1β (10 μg per mouse, i.p.) was injected twice a week [25]. At the end of the experiment, body and liver weights were determined and serum samples were collected. Serum lipid triglycerides (TGs), total cholesterol (TC), alanine transaminase (ALT) and aspartate aminotransferase (AST) were measured by using the kits purchased from Nanjing Jiancheng Bioengineering institute according to the manufacturer's protocols.

2.3. Histological staining

The paraffin-embedded liver sections were stained with hematoxylin and eosin (H&E) and oil red O staining was used to visualize the pattern of lipid accumulation using frozen liver sections. Masson and Sirius Red staining were used to detect the fibrosis. Immunohistochemical (IHC) staining and immunofluorescence (IF) were described in the supplementary materials. Histological images were obtained using a light microscope.

2.4. Detection of ROS in tissues

The liver tissues staining of ROS was detected by dihydroethidium (DHE). Briefly, cryosections were incubated with 10 μM DHE at 37 °C for 30 min. Fluorescence was detected by a fluorescence microscope system.

2.5. Transmission electron microscope (TEM)

The liver tissues were prefixed with 3 % glutaraldehyde, and were postfixed in 1 % osmium tetroxide, dehydrated in series acetone, infiltrated in Epox 812 for a longer, and embedded. The semithin sections were stained with methylene blue and ultrathin sections were cut with diamond knife, stained with uranyl acetate and lead citrate. Sections were examined with JEM-1400-FLASH Transmission Electron Microscope.

2.6. Measurement of mitochondrial membrane potential (Ψm)

TMRM (#T668, Life Technologies) was used to measure mitochondrial membrane potential (Ψm) according to manufacturer's instructions. Briefly, transfected cells were primed with PA for 4 h. Cells were stained with 200 nM TMRM for 30 min at 37 °C and then treated with CCCP (5 mM) for 5 min. After washing twice, fluorescence intensity was determined using a FilterMax F5 multimode plate reader.

More details about the methods and materials are available in the Supplementary Materials.

3. Results

3.1. Hepatic expression of SLC7A11 is upregulated in NASH patients and positively correlates with disease severity

To determine the involvement of SLC7A11 in NAFLD and NASH, we first measured SLC7A11 expression in liver samples from patients with NAFLD and NASH, as well as control subjects. Both mRNA and protein levels of SLC7A11 were significantly upregulated in patients with NASH compared to patients with NAFLD and with normal liver tissues (Fig. 1A-B). The IHC staining of SLC7A11 also proved these results (Fig. 1C). We next documented the clinical importance of SLC7A11 expression. To explore the clinical relevance of SLC7A11 expression, we divided NASH patients into two groups according to the median value of SLC7A11 detected by RT-qPCR: SLC7A11 high expression (15/30) and SLC7A11 low expression (15/30). According to the histological staining, we found that the liver tissues with higher SLC7A11 expression had more hepatic

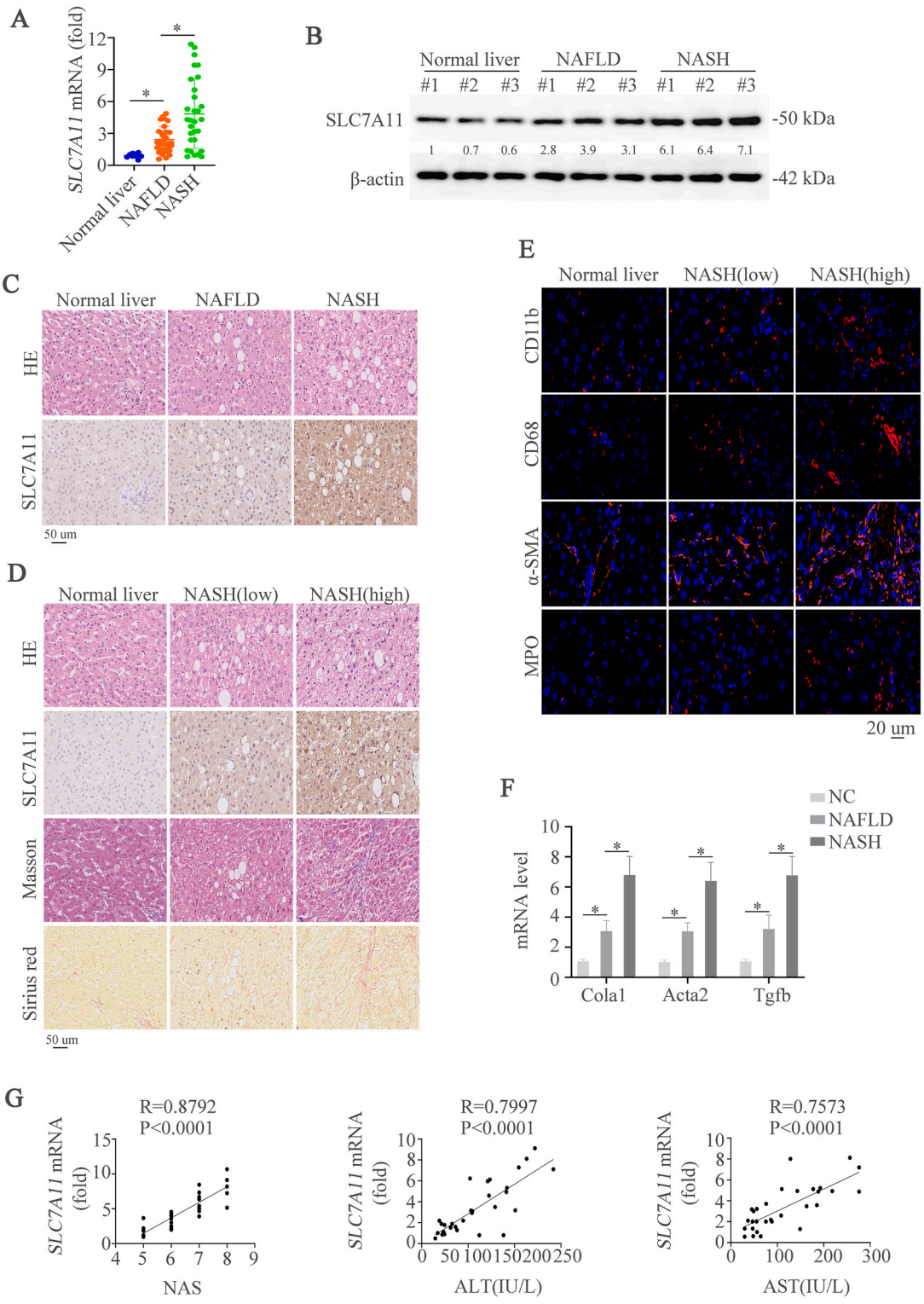

Fig. 1. Hepatic expression of SLC7A11 is upregulated in NASH patients and positively correlates with disease severity
(A) *SLC7A11* mRNA levels in liver tissues of human normal controls (n = 10), non-alcoholic fatty liver disease (NAFLD) (n = 30), and NASH (n = 30) as determined by RT-qPCR. (B) Western blot was used to show the expression level of SLC7A11 protein in liver extracts from patients with normal controls, NAFLD and NASH. (C) Representative hematoxylin and Eosin (HE) and immunohistochemistry (IHC) images of control, NAFLD, and NASH liver sections were shown. Scale bars indicate 50 μm. (D) HE, SLC7A11 expression by IHC, Masson staining and Sirius Red in liver sections from normal controls, NAFLD and NASH. Scale bars indicate 50 μm. (E) Representative IF staining showed CD11b, CD68, α-SMA and myeloperoxidase (MPO). Scale bars indicate 20 μm. (F) The mRNA levels of *Cola1*, *Acta2* and *Tgfb* in liver tissues of human normal controls, non-alcoholic fatty liver disease, and NASH (n = 30) as determined by RT-qPCR. (G) The correlation between *SLC7A11* mRNA levels and NAS, serum ALT and AST levels in patients with NASH. *p < 0.05. (For interpretation of the references to colour in this figure legend, the reader is referred to the Web version of this article.)

lipid accumulation, worse fibrosis, more infiltration of inflammatory cells, and more serious liver damage (Fig. 1D-G). Overall, these data demonstrate the importance of SLC7A11 in human liver during progression from normal to NAFLD and NASH.

3.2. *Upregulated SLC7A11 level is shown in mouse NASH models and hepatic SLC7A11 deficiency deteriorates diet-induced NASH*

In order to detect the expression of SLC7A11 in mouse NASH models, we first established two NASH mouse models by treating the mice with

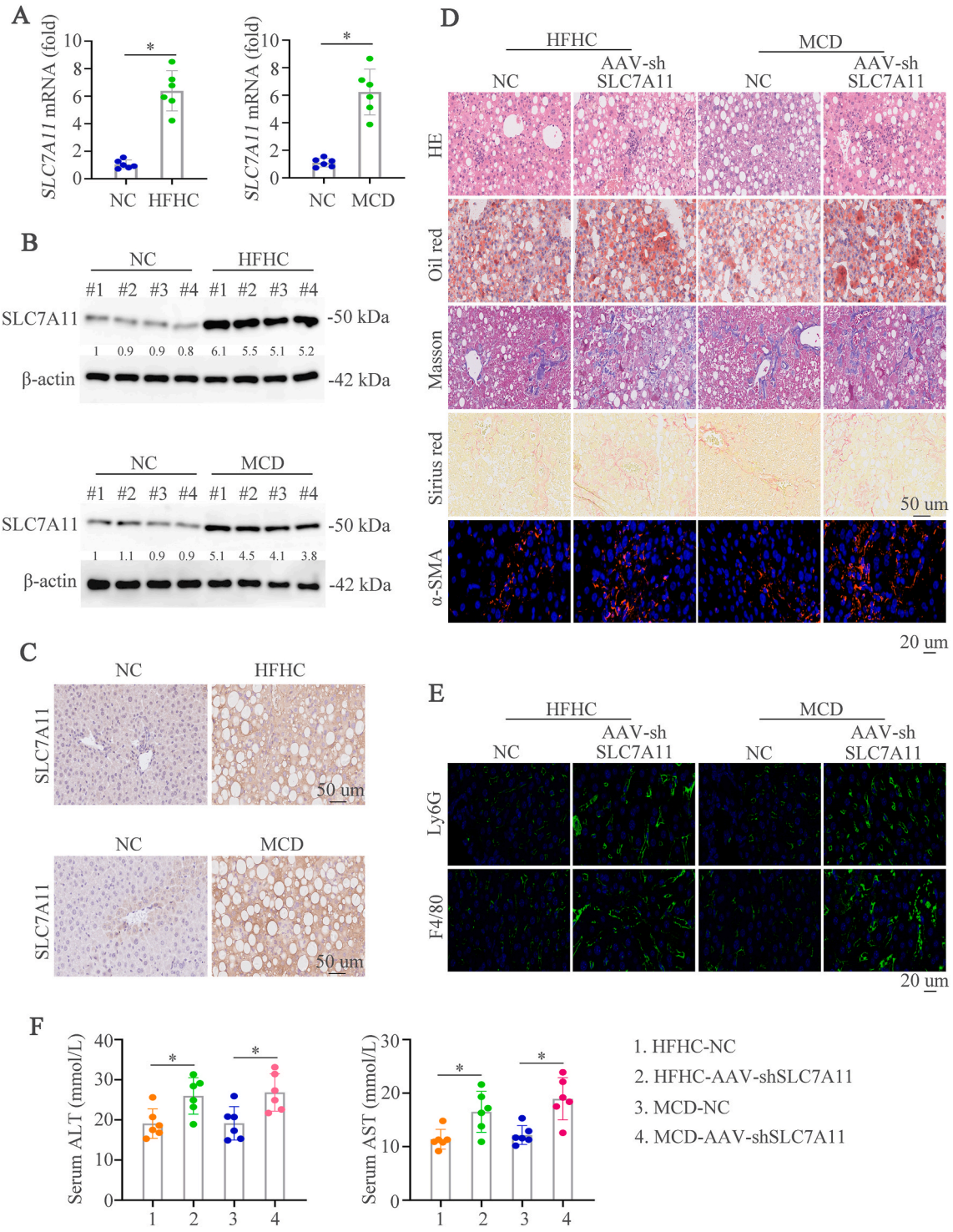

Fig. 2. Upregulated SLC7A11 level is shown in mouse NASH models and hepatic SLC7A11 deficiency deteriorates diet-induced NASH
(A) Hepatic mRNA level of *SLC7A11* in wildtype (WT) mice fed the normal chow, HFHC, or MCD diet. (B) Protein levels in wildtype (WT) mice fed the normal chow, HFHC, or MCD diet. (C) IHC showed the SLC7A11 expression in indicated mice groups. (D) HE, Oil Red O, Masson, Sirius Red, and α-SMA staining were shown in WT or SLC7A11 knockdown mice fed with HFHC, or MCD diet. (E) Representative IF staining showed Ly6G and F4/80. (F) Graphs showed the serum ALT and AST in mice (n = 6/group). Scale bars indicate 50 μm for IHC and 20 μm for IF. Error bars represent mean ± SD. *p < 0.05. (For interpretation of the references to colour in this figure legend, the reader is referred to the Web version of this article.)

HFHC for 28 weeks [21] or MCD for 8 weeks [22], and we found that hepatic SLC7A11 expression was elevated in NASH mouse models induced by HFHC or MCD diets (Fig. 2A-C). The immunofluorescence staining of SLC7A11 and Albumin demonstrated that higher SLC7A11 expression in hepatocytes from NASH mice than control mice (Supplementary Fig. 1A). We then knockdown the expression of SLC7A11 by AAV (AAV-shSLC7A11) to assess its role in NASH. Firstly, we found that AAV-shSLC7A11 could decrease the SLC7A11 expression compared to AAV-shcontrol mice group with normal chow (NC). However, liver weight, TG and cholesterol levels had no significant effect between AAV-shSLC7A11 and AAV-shcontrol group (Supplementary Fig. 1B). 8-week-old mice were fed a HFHC diet or a MCD diet and then treated

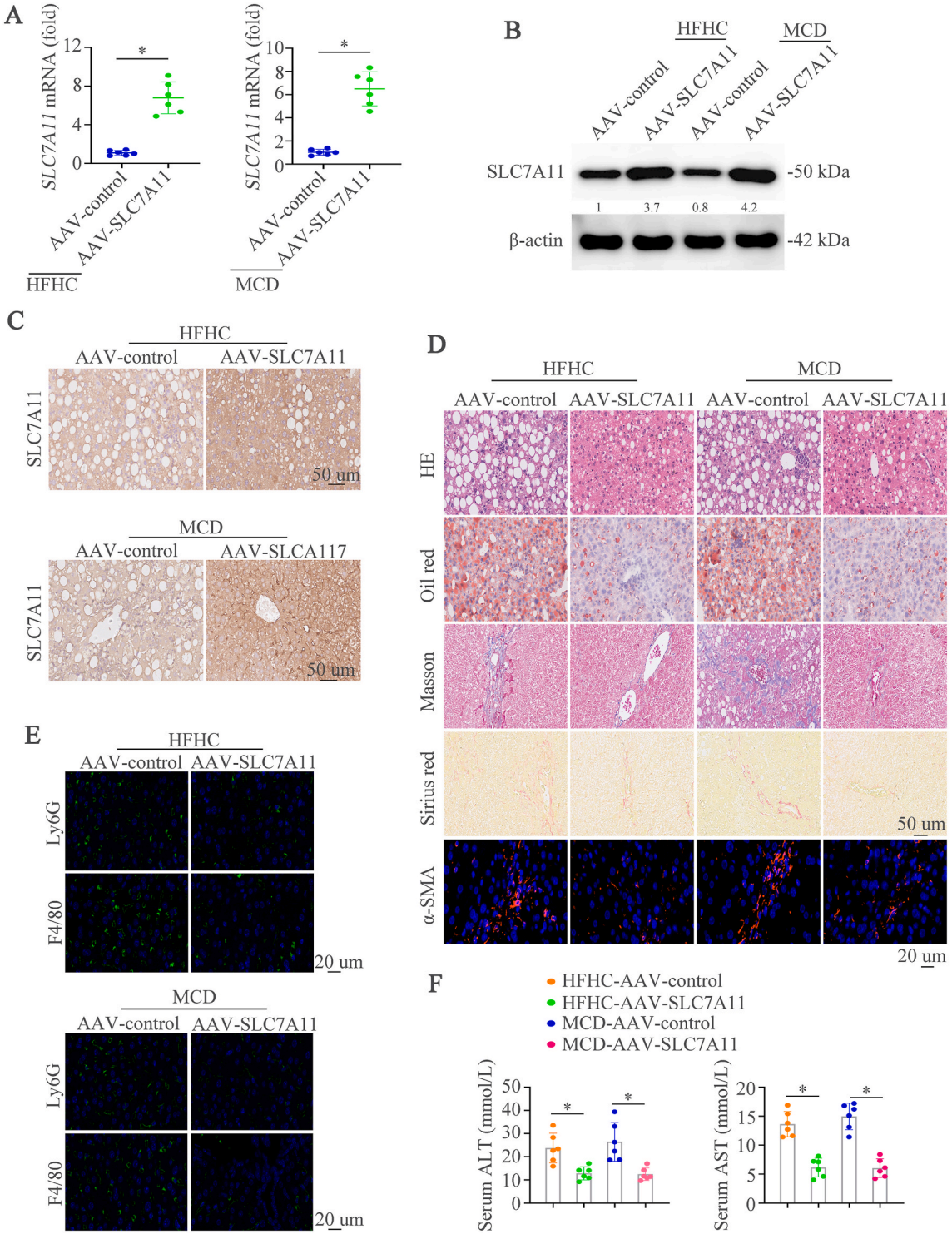

Fig. 3. Hepatocyte-specific overexpression of SLC7A11 aggravates NASH
(A-C) Hepatic mRNA (A), protein levels (B) and IHC staining (C) of SLC7A11 in AAV-control or AAV-SLC7A11 mice fed with HFHC, or MCD diet. (D) HE, Oil Red O, Masson, Sirius Red, and α-SMA staining were shown in AAV-control or AAV-SLC7A11 mice fed with HFHC, or MCD diet. (E) Representative IF staining showed Ly6G and F4/80. (F) Graphs showed the serum ALT and AST in mice (n = 6/group). Scale bars indicate 50 μm for IHC and 20 μm for IF. Error bars represent mean ± SD. *p < 0.05. (For interpretation of the references to colour in this figure legend, the reader is referred to the Web version of this article.)

with AAV-shcontrol or AAV-shSLC7A11 to gain the NASH models with SLC7A11 knockdown. Hematoxylin and Eosin (HE), Oil Red O, Masson, Sirius Red, and IF staining of α-SMA showed that SLC7A11 deficiency aggravated hepatic lipid accumulation, inflammation, and fibrosis (Fig. 2D). Macrophages and neutrophils are proved to main myeloid cells involved in NASH progression [26,27]. Therefore, macrophages (F4/80) and neutrophils (Ly6G) were detected to evaluate the function of SLC7A11 in NASH progression. We found significantly increased numbers of infiltrated inflammatory macrophages and neutrophils in SLC7A11 knockdown mice compared to control mice as detected by IF (Fig. 2E). Furthermore, SLC7A11 knockdown in consistently augmented liver enzymes was shown by ALT and AST (Fig. 2F). Liver weight, TG and cholesterol levels were increased in SLC7A11 knockdown NASH mice (Supplementary Fig. 1C). Moreover, SLC7A11 knockout mice were used to check its influence on NASH progression and we found that SLC7A11 knockout contributed to hepatic lipid accumulation, inflammation, and fibrosis (Supplementary Figs. 1D–1F). These data illustrate that hepatic knockdown or knockout of SLC7A11 deteriorate liver inflammation and liver damage in NASH mouse models.

3.3. Hepatocyte-specific overexpression of SLC7A11 improves NASH

To further investigate the function of SLC7A11 in NASH in *vivo*, we constructed an overexpression of SLC7A11 mouse model by applying the AAV (AAV-SLC7A11). Firstly, we found that AAV-SLC7A11 could increase the SLC7A11 expression compared to AAV-control mice group with normal chow (NC). However, liver weight, TG and cholesterol levels had no significant effect between AAV-SLC7A11 and AAV-control group (Supplementary Fig. 2A). The overexpression of SLC7A11 was confirmed by RT-qPCR, western blot and IHC in NASH models (Fig. 3A-C). Hepatic SLC7A11 overexpression and littermate mice were subjected to feed with HFHC or MCD diet. HE, Oil Red O, Masson, Sirius Red, and IF staining of α-SMA showed that SLC7A11 overexpression decreased hepatic lipid accumulation, inflammation, and fibrosis (Fig. 3D). In addition, we also found significantly reduced numbers of infiltrated macrophages and neutrophils in AAV-SLC7A11 mice compared to AAV-control mice as detected by IF (Fig. 3E). Furthermore, mice with SLC7A11 upregulation had ameliorative liver enzymes (Fig. 3F). Liver weight, TG and cholesterol levels were largely increased in SLC7A11 upregulation mice (Supplementary Figs. 2B–2D). These data illustrate that the important roles of hepatic SLC7A11 in against liver inflammation and liver damage in NASH mouse models.

3.4. SLC7A11 promotes the activation of AMPK pathway and impairs NASH progression

In order to detect the mechanism of SLC7A11 in regulating NASH progression, we performed RNA sequencing analysis by using the liver tissues of HFHC-AAV-control and HFHC-AAV-SLC7A11. The Metascape and Kyoto Encyclopedia of Genes and Genomes (KEGG) pathway analysis identified largely changed pathways between HFHC-AAV-control and HFHC-AAV-SLC7A11. The AMPK pathway was the most significant changed axis in these pathways (Fig. 4A and B). To prove the roles of AMPK pathway in SLC7A11-regulated NASH, we firstly examined the AMPK Thr172 phosphorylation (pAMPK) which indicated activation of AMPK in livers of NASH mice models. The results demonstrated that pAMPK expression was decreased in NASH liver tissues (Fig. 4C and Supplementary Fig. 3A), and the expression of pAMPK weaken further when SLC7A11 was knocked down (Fig. 4D and Supplementary Fig. 3B), indicating repression of AMPK activity. However, the upregulation of SLC7A11 augmented pAMPK level shown by western blot and IHC (Fig. 4E-F and Supplementary Figs. 3C–3D). The in *vitro* analysis by using Hepa1-6 cells also confirmed that SLC7A11 could rescue the expression of pAMPK (Supplementary Fig. 3E). In order to further study the role of AMPK in SLC7A11-regulated NASH, we treated the AAV-SLC7A11 NASH mice with or without AMPK inhibitor compound C (CC) [28,29]. HE, Oil Red O, Masson, Sirius Red, and IF staining of α-SMA illustrated that AMPK inhibition by CC aggravated hepatic lipid accumulation, inflammation, and fibrosis (Fig. 4G). We also found significantly increased numbers of infiltrated inflammatory immune cells in mice with CC compared to control mice as shown by F4/80 and Ly6G (Fig. 4H). ELISA also confirmed that AMPK inhibition could aggravate liver damage in AAV-SLC7A11 NASH mice (Supplementary Fig. 3F). AMPK is a key metabolic regulator that senses energy status and controls energy expenditure and storage, which attenuates NASH progression [30–32]. Therefore, according to the above results, we find that SLC7A11 might impair NASH progression by activating AMPK pathway.

3.5. SLC7A11 activates AMPK pathway by decreasing ROS level and promoting αKG/PHD activity

SLC7A11-mediated cystine uptake promotes GSH synthesis, which is indispensable to scavenge excessive ROS [33,34]. ROS signaling deactivates AMPK pathway [35,36]. Therefore, we hypothesized that SLC7A11 might activate AMPK through decreasing ROS. The ROS staining demonstrated that HFHC diet could increase ROS level and SLC7A11 knockdown sharply increased the ROS. However, the reduced ROS staining was found when SLC7A11 was upregulated (Fig. 5A). These works were confirmed in *vitro* analysis, which demonstrated that SLC7A11 could attenuate ROS level induced by palmitic acid (PA), and SLC7A11 knockdown largely augmented ROS level (Fig. 5B). N-acetyl-L-cysteine (NAC), a broadly used ROS scavenger [37,38], accelerated pAMPK expression in Hepa1-6-shSLC7A11 cells with PA treatment (Fig. 5C). These results illustrate that SLC7A11 could regulate AMPK activation by decreasing ROS level.

Our previous study also found that SLC7A11 could decrease αKG content [15]. We conjected that SLC7A11 might influence AMPK pathway by αKG. In NASH models, SLC7A11 downregulation could increase αKG content and upregulated SLC7A11 had the reversed effect (Fig. 5D). Similar results were confirmed in *vitro* experiments (Fig. 5E). Further, dimethyl-αKG (DM-αKG), a cell-permeable analog of αKG suppressed AMPK Thr172 phosphorylation induced by SLC7A11 in PA-treated Hepa1-6 cells (Fig. 5F). Because αKG can interfere with cellular function by activating PHD enzymes [39]. We examined whether αKG suppressed AMPK pathway activation in a PHD-dependent manner. Treatment with dimethyloxalylglycine (DMOG), an inhibitor of PHD activity, restored pAPMK expression reduced by DM-αKG in PA-treated Hepa1-6-SLC7A11 cells (Fig. 5G). To further assess the roles of αKG in SLC7A11-induced protective function in NASH, the DM-αKG was applied in NASH mice with AAV-SLC7A11. HE, Oil Red O, Masson, Sirius Red, and IF staining of α-SMA demonstrated that the addition of DM-αKG blocked the protective role of SLC7A11 and showed by aggravated hepatic lipid accumulation, inflammation, and fibrosis (Fig. 5H). In addition, we also found significantly increased numbers of infiltrated immune cells and aggravated liver damage in DM-αKG-treated mice compared to controls (Fig. 5I, Supplementary Fig. 3G). These data suggest that αKG impairs AMPK activation by augmenting PHD activity and deteriorates NASH.

3.6. SLC7A11 impairs the expression of NLRP3 inflammasome components by AMPK-induced mitophagy

The above works in Fig. 4B also found that NOD-like receptor signaling pathway was vital in SLC7A11-treated NASH. NOD-, LRR- and pyrin domain-containing 3 (NLRP3) is the best characterized cytosolic nod-like pattern recognition receptor [40,41], which is activated in NASH and promotes liver fibrosis and NASH progression [42,43]. We first analyzed the inflammatory cytokines in NASH models and found that inflammasomes mediators IL-1β and IL-18 ($P < 0.01$) were significantly upregulated when SLC7A11 was knockdown (Fig. 6A). However, SLC7A11 upregulation could reverse the mRNA levels of IL-1β and IL-18 (Supplementary Fig. 4A). Similarly, IL-1β was increased in liver tissues

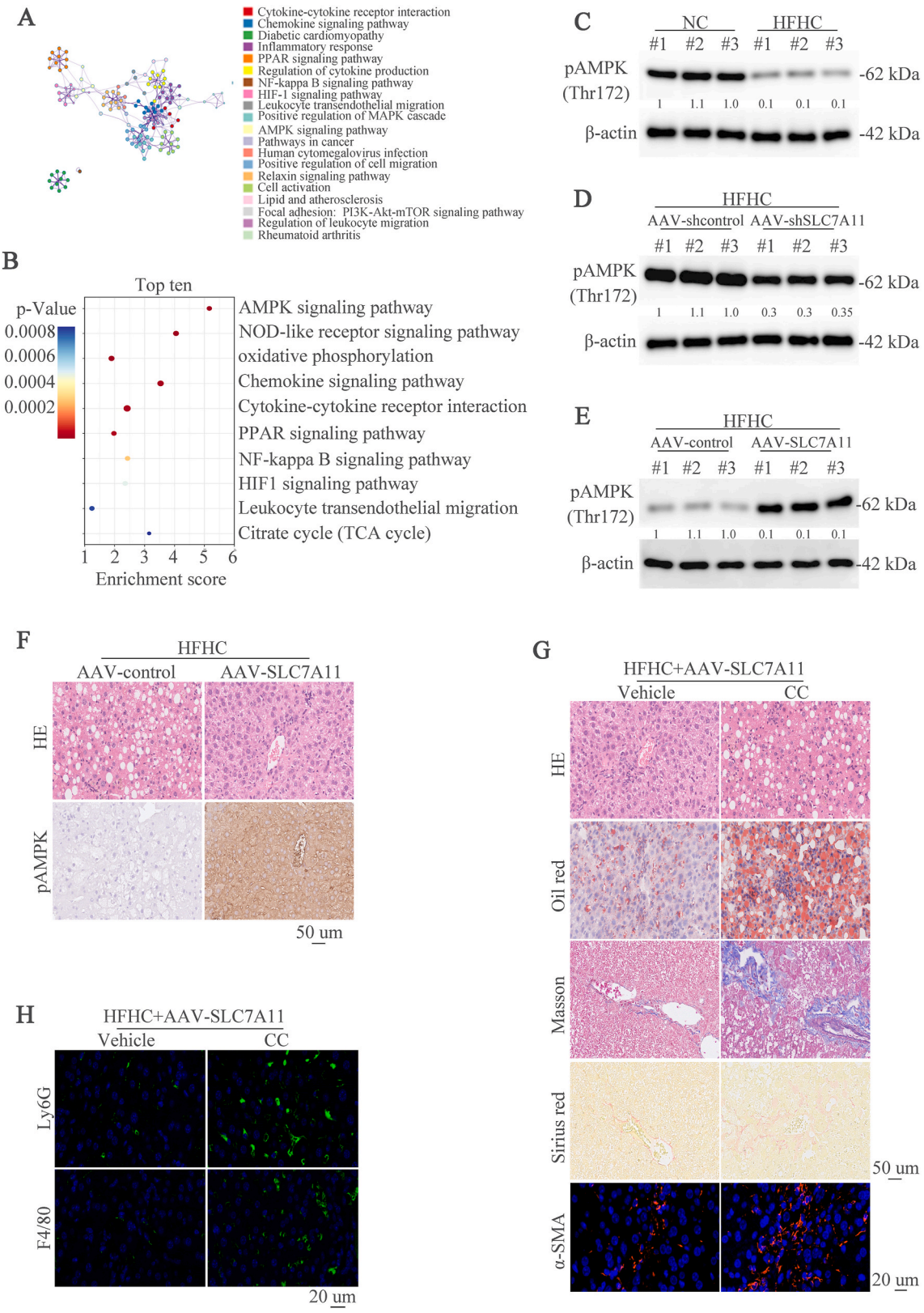

Fig. 4. SLC7A11 promotes the activation of AMPK pathway and impairs NASH progression
(A-B) The Metascape (A) and Kyoto Encyclopedia of Genes and Genomes (KEGG) (B) identified changed pathways between HFHC-AAV-control and HFHC-AAV-SLC7A11. (C) Western blot showed the pAMPK (Thr172) expression in mice with normal chow and HFHC diet. (D) Western blot showed the pAMPK (Thr172) expression in HFHC diet mice with shcontrol or shSLC7A11. (E) Western blot showed the pAMPK (Thr172) expression in mice with control or SLC7A11 upregulation and treated with HFHC diet. (F) HE and pAMPK staining were exhibited in AAV-control or AAV-SLC7A11 mice fed with HFHC diet. (G) Mice with SLC7A11 upregulation treated with HFHC diet. Then, mice were given with control or AMPK inhibitor CC. n = 6 per group. HE, Oil Red O, Masson, Sirius Red, and α-SMA staining were demonstrated in 2 groups of mice. (H) Representative IF staining showed Ly6G and F4/80 in 2 groups of mice. (For interpretation of the references to colour in this figure legend, the reader is referred to the Web version of this article.)

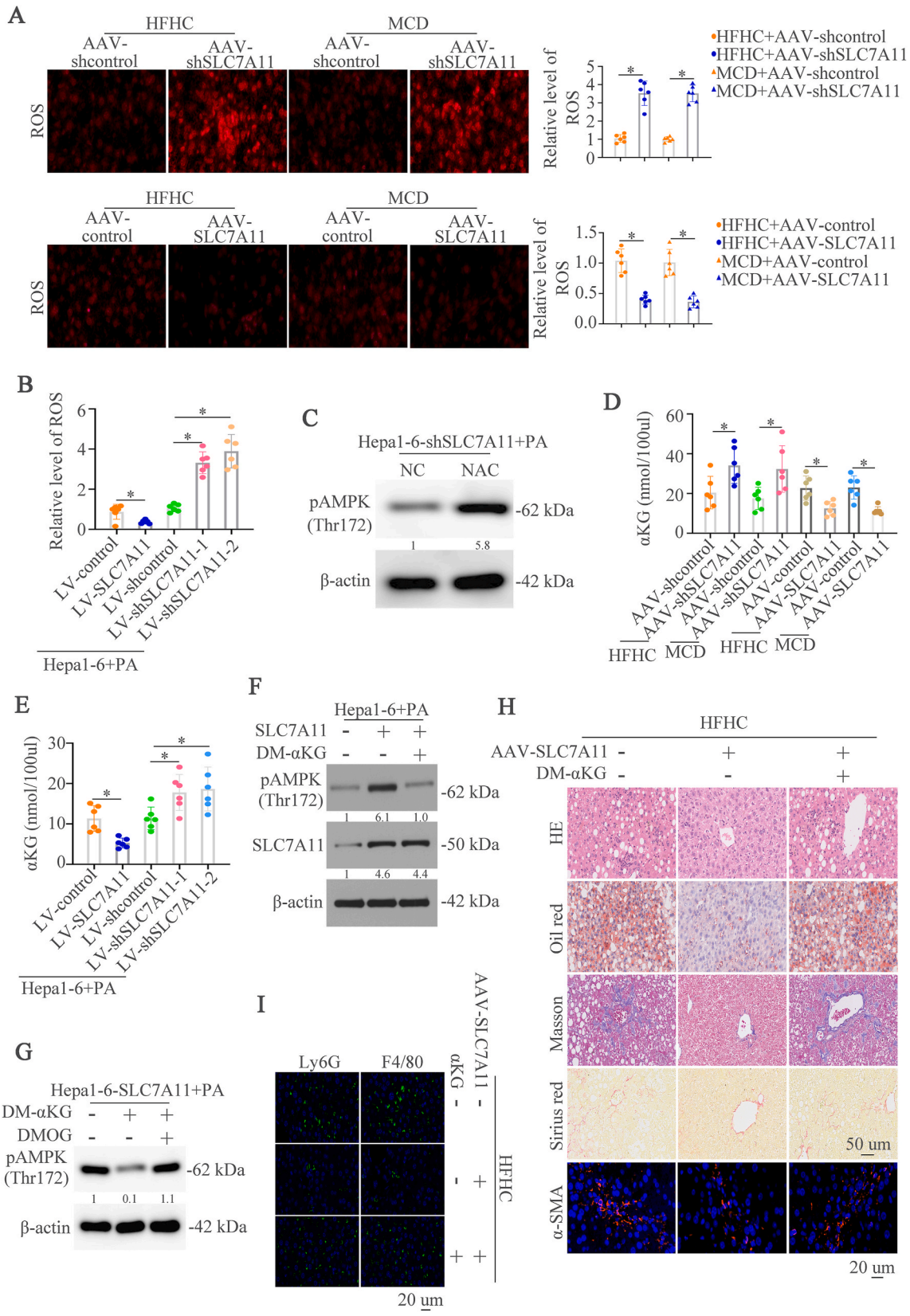

(caption on next page)

Fig. 5. SLC7A11 activates AMPK pathway by decreasing ROS level and promoting αKG/PHD activity
(A) Representative images of ROS staining in liver tissues in NASH mice with SLC7A11 knockdown or upregulation. (B) Hepa1-6 cells transfected with LV-control, LV-SLC7A11, LV-shcontrol, LV-shSLC7A11-1 and LV-shSLC7A11-2 lentivirus and then treated with PA. ROS staining was detected in these groups. (C) Hepa1-6-shSLC7A11 cell were treated with control or N-acetyl-L-cysteine (NAC) and followed by PA. Western blot showed the pAMPK (Thr172) expression. (D) αKG content was measured in NASH mice with SLC7A11 downregulation or SLC7A11 downregulation. (E) Hepa1-6 cells transfected with LV-control, LV-SLC7A11, LV-shcontrol, LV-shSLC7A11-1 and LV-shSLC7A11-2 lentivirus and then treated with PA. αKG content was measured in these groups. (F) Hepa1-6 cells transfected with LV-control and LV-SLC7A11 lentivirus and then treated with or without dimethyl-αKG (DM-αKG) followed by PA. Western blot showed the pAMPK (Thr172) and SLC7A11 expression. (G) Hepa1-6-SLC7A11 cells treated with DM-αKG alone or DM-αKG and dimethyloxalylglycine (DMOG) and followed by PA. Western blot showed the pAMPK (Thr172) expression. (H) Mice with or without SLC7A11 upregulation fed with HFHC diet and then treated with control or DM-αKG. n = 6 per group. HE, Oil Red O, Masson, Sirius Red, and α-SMA staining were demonstrated in these groups of mice. (I) Representative IF staining showed Ly6G and F4/80 in these groups of mice. (For interpretation of the references to colour in this figure legend, the reader is referred to the Web version of this article.)

and serum under SLC7A11 knockdown in NASH models (Fig. 6B) and increased-SLC7A11 expression could abolish IL-1β upregulation in these samples (Supplementary Fig. 4B). Western blot analysis revealed that active NLRP3 inflammasome components such as mature IL-1β and cleaved caspase-1 was upregulated when SLC7A11 was knocked down. However, SLC7A11 upregulation decreased the expression of NLRP3 inflammasome components (Fig. 6C). These works demonstrated that SLC7A11 might inhibit NLRP3 inflammasome expression.

We next tried to determine how SLC7A11 regulated NLRP3 expression. Because SLC7A11 could activate AMPK, we hypothesized that SLC7A11 could regulate NLRP3 expression through AMPK. Knocking down AMPKα1, the predominant catalytic subunit, showed enhanced NLRP3 expression, caspase-1 cleavage and IL-1β release (Fig. 6D, Supplementary Fig. 4C). As expected, inhibition of AMPKα1 enhanced caspase-1 activity decreased by SLC7A11 upregulation in PA-treated Hepa1-6 cells (Supplementary Fig. 4D). Consistently, AMPK activation by the selective AMPK agonist A769662 significantly reduced IL-1β production (Supplementary Fig. 4E). IHC staining showed that AMPK inhibition by CC significant decreased expression of cleaved caspase-1 and mature IL-1β (Fig. 6E). Above works illustrate that SLC7A11 impairs NLRP3 inflammasome expression by AMPK pathway.

AMPK activation stimulates autophagy/mitophagy via phosphorylation of ULK1 and mitochondrial fission factor (MFF), a mitochondrial outer-membrane receptor for DRP1 [44,45]. DRP1 binds to fission sites, which isolate mitochondria with reduced membrane potential, thereby enhancing recruitment of the mitophagy-promoting E3 ubiquitin ligase Parkin [46]. Upregulation of SLC7A11 reduced mitochondrial membrane potential (Ψm) and knockdown of SLC7A11 had opposite effect at least as effectively as the uncoupler carbonyl cyanide *m*-chlorophenyl hydrazone (CCCP) (Fig. 6F). Knocking down AMPKα1 could reverse the reduced mitochondrial membrane potential caused by SLC7A11 upregulation (Fig. 6G). Transmission electron microscope (TEM) exhibited that AMPKα1 knockdown could decrease the mitophagy (Fig. 6H). Western blot showed that AMPKα1 knockdown decreased the expression of Drp1 and P62, suggesting decreased mitophagy. Mitophagy leads to decrease damaged mitochondria producing ROS and oxidized cytosolic mitochondrial DNA, which in turn blocks NLRP3 inflammasome overactivation and expression [47,48]. All of these works suggest that SLC7A11 inhibits NLRP3 inflammasome by AMPK-induced mitophagy.

3.7. Inhibition of IL-1β pathway by neutralizing Abs or anakinra improves SLC7A11 knockdown-induced liver fibrosis and NASH progression

Inflammation is an important characteristic in NASH and IL-1β could induce NASH progression [42,49,50]. IL-1β was used to stimulate primary hepatic stellate cells (HSCs) which is responsible for liver fibrosis and found that IL-1β could increase expression of α-SMA and Collagen-1 in a dose-dependent manner (Fig. 7A). Treating HSCs cells with supernatant of PA-treated Hepa1-6-shSLC7A11 cells and then given with control or IL-1β neutralizing Abs (Anti-IL-1β), the western blot found that anti-IL-1β could decrease the expression of α-SMA and Collagen-1 (Fig. 7B). Our above works have demonstrated that SLC7A11 could regulate immune cells infiltration and IL-1β could also recruit immune cells [15,25]. Therefore, we conjectured that SLC7A11 knockdown might recruit immune cells by IL-1β. We first examined the effect of IL-1β on the motility of bone-marrow–derived macrophages (BMDMs) and found that IL-1β dramatically increased the migrative capacity of BMDMs (Fig. 7C). The conditioned medium from PA-stimulated Hepa1-6-shSLC7A11 cells was used to culture BMDMs and simultaneously gave cells anti-IL-1β or IL-1R1 antagonist anakinra. The results showed that anti-IL-1β and anakinra could largely decrease the conditioned medium-induced BMDMs migration (Fig. 7D).

We then evaluated the effect of anti-IL-1β and anakinra on SLC7A11 knockdown-induced NASH in *vivo* by using two NASH models. HE, Oil Red O, Masson, Sirius Red, and IF staining of α-SMA demonstrated that anti-IL-1β and anakinra improved hepatic lipid accumulation, inflammation, and fibrosis, which were deteriorated by SLC7A11 knockdown (Fig. 7E and Supplementary Fig. 5A). In addition, we also found significantly decreased numbers of infiltrated immune cells in anti-IL-1β or anakinra-treated mice compared to controls (Fig. 7F, Supplementary Fig. 5B). Liver enzymes, TG and cholesterol levels were decreased in anti-IL-1β or anakinra-treated mice (Fig. 7G, Supplementary Figs. 5C–5D). These data demonstrates that inhibition of IL-1β pathway could effectively block liver fibrosis and NASH progression caused by SLC7A11 knockdown.

3.8. Lipid-induced JNK-c-Jun pathway contributes to the upregulation of SLC7A11 in NASH

Our above works found that SLC7A11 was upregulated in NASH. Therefore, we hypothesized that lipid might be a contributor to SLC7A11 upregulation. RT-qPCR and western blot analysis showed that PA could upregulate SLC7A11 expression (Fig. 8A-B). Moreover, PA treatment increased the promoter activity of SLC7A11 (Fig. 8C). To define the roles of the *cis*-regulatory elements of the SLC7A11 promoter in response to PA treatment, a series of truncated mutants of the SLC7A11 promoter were generated. A deletion from nt-847 to −373 significantly decreased PA-induced SLC7A11 promoter activity, hinting that this sequence was vital for the activation of the SLC7A11 promoter induced by PA. Three transcription factors binding sites were located in this region. Site-directed mutagenesis showed that mutation of c-Jun binding site significantly reduced SLC7A11 promoter activity induced by PA (Fig. 8D). A ChIP assay confirmed that c-Jun could bind to the SLC7A11 promoter (Fig. 8E).

Luciferase activity and RT-qPCR analysis demonstrated that knockdown of c-Jun impaired the SLC7A11 promoter activity and decreased the mRNA level of SLC7A11 regulated by PA (Fig. 8F-G). Western blot demonstrated that c-Jun knockdown decreased PA-induced SLC7A11 expression (Fig. 8H). To characterize which signaling pathway mediated PA-dependent SLC7A11 induction, Hepa1-6 cells were simultaneously treated with PA and inhibitors of extracellular signal-regulated kinase (ERK), p38, JNK, or PI3K pathways. JNK inhibitor largely abolished PA-mediated SLC7A11 induction, whereas other kinase inhibitors had little effect (Fig. 8I). These studies suggested that lipid upregulated SLC7A11 expression through JNK-c-Jun pathway.

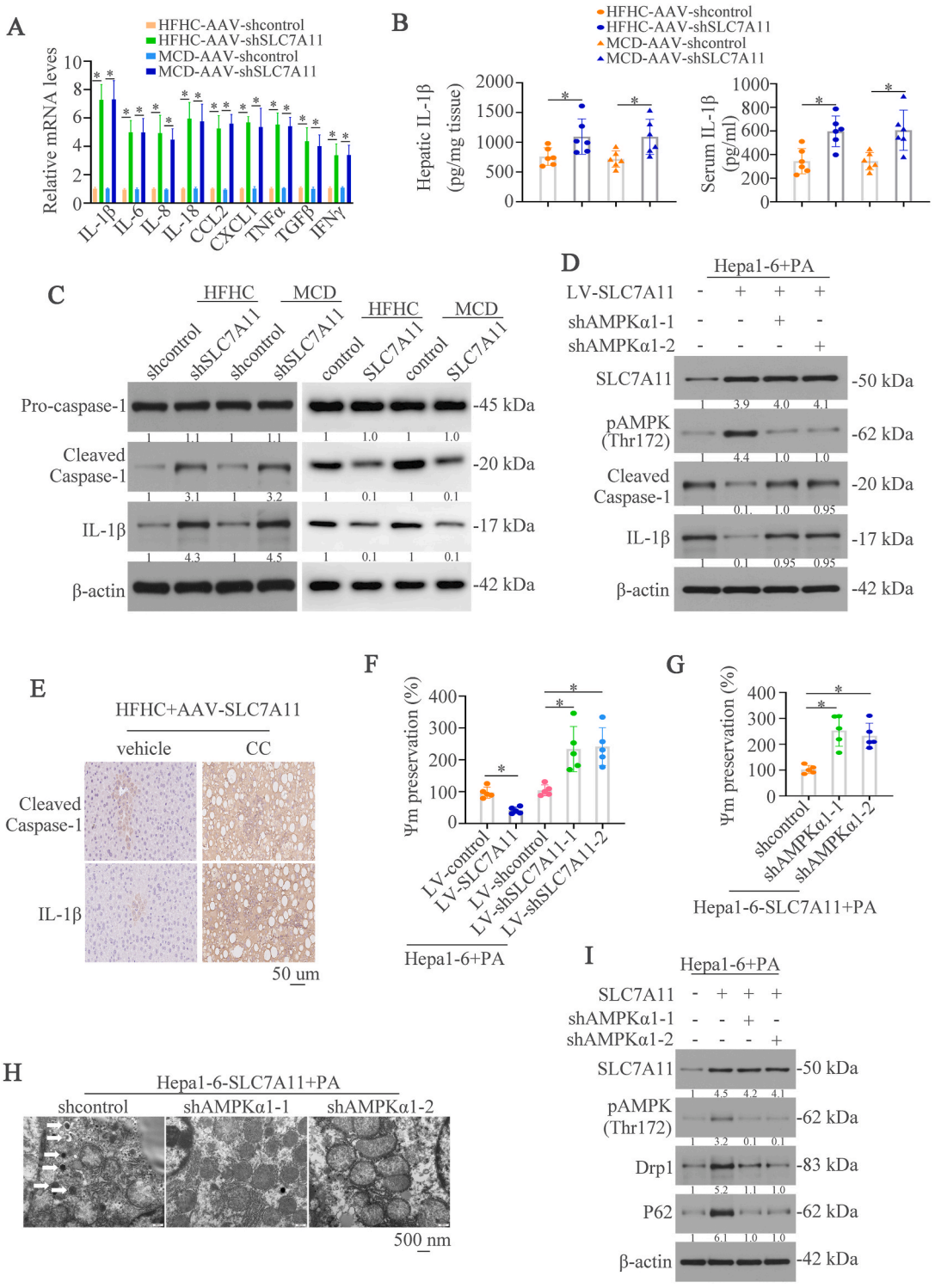

Fig. 6. SLC7A11 impairs the expression of NLRP3 inflammasome components by AMPK-induced mitophagy
(A) mRNA levels in AAV-shcontrol or AAV-shSLC7A11 mice fed with HFHC, or MCD diet. (B) IL-1β expression in hepatic tissues and serum in AAV-shcontrol or AAV-shSLC7A11 mice fed with HFHC, or MCD diet. (C) Western blot demonstrated the expression of pro-caspase-1, cleaved-caspase-1 and IL-1β in AAV-shcontrol, AAV-shSLC7A11, AAV-control and AAV-SLC7A11 mice fed with HFHC, or MCD diet. (D) Hepa1-6 cells transfected with LV-SLC7A11 or cotransfected with LV-SLC7A11 and LV-shAMPKα1-1/LV-shAMPKα1-2. Western blot demonstrated the expression of SLC7A11, pAMPK (Thr172), cleaved-caspase-1 and IL-1β. (E) Mice with SLC7A11 upregulation were treated with HFHC diet. Then, mice were given with control or AMPK inhibitor CC. n = 6 per group. IHC showed the expression of cleaved-caspase-1 and IL-1β. (F) Hepa1-6 cells transfected with LV-control, LV-SLC7A11, LV-shcontrol, LV-shSLC7A11-1 and LV-shSLC7A11-2 lentivirus and then treated with PA. Mitochondrial membrane potential was measured in these groups. (G) Hepa1-6-SLC7A11 cells transfected with LV-shcontrol, LV-shAMPKα1-1/LV-shAMPKα1-2 and then treated with PA. Mitochondrial membrane potential was measured in these groups. (H) Transmission electron microscope (TEM) exhibited mitophagy in these cells. (I) Western blot demonstrated the expression of SLC7A11, pAMPK (Thr172), Drp1 and P62 in indicated groups.

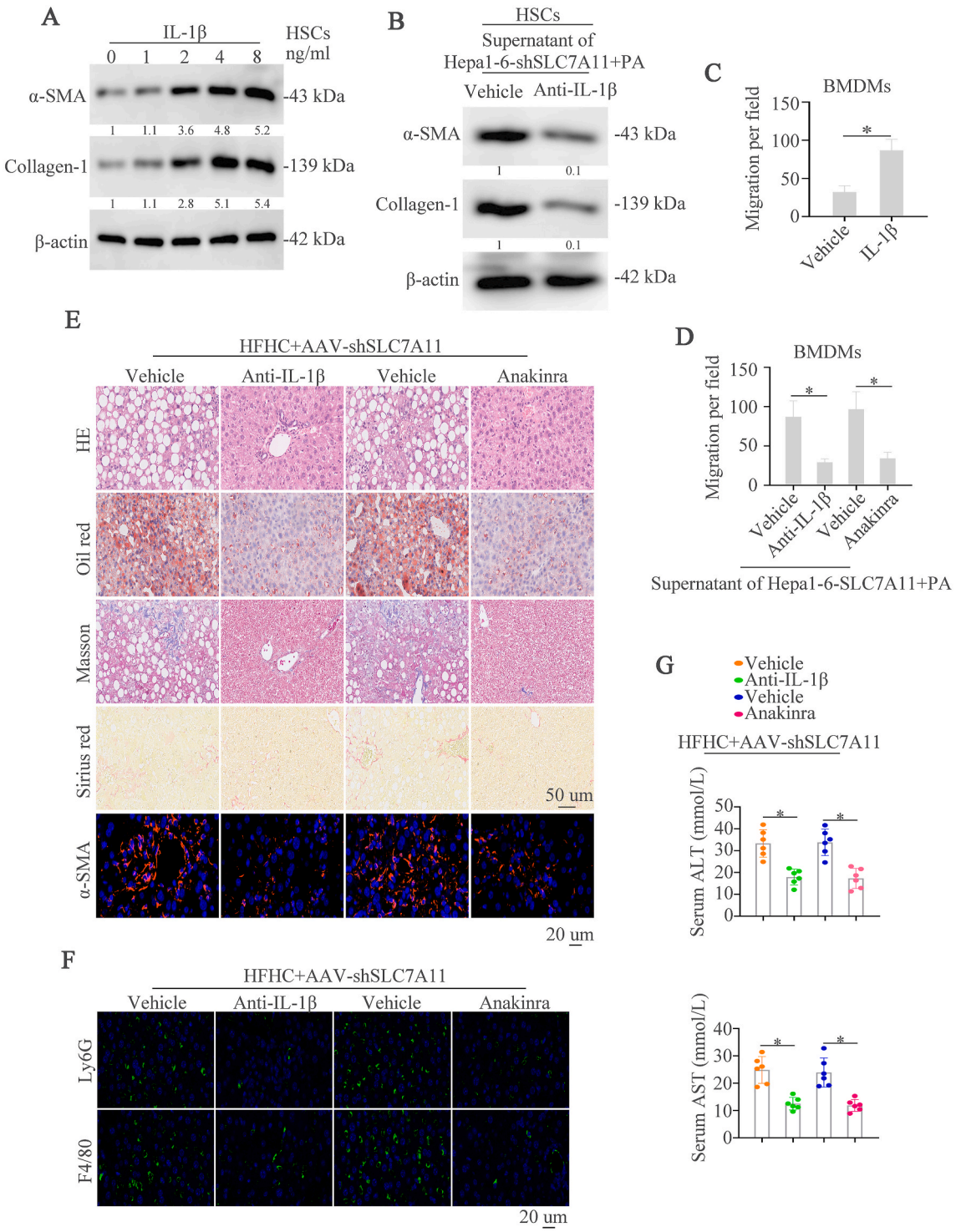

Fig. 7. Inhibition of IL-1β pathway by neutralizing Abs or anakinra improves SLC7A11 knockdown-induced liver fibrosis and NASH progression
(A) Primary hepatic stellate cells (HSCs) were treated with different concentration of IL-1β. Western blot demonstrated the expression of α-SMA and Collagen-1. (B) HSCs were given with the supernatant of Hepa1-6-SLC7A11 with the stimulation of PA and then vehicle or anti-IL-1β were added to HSCs. Western blot showed the expression of α-SMA and Collagen-1. (C) The migrative ability of BMDMs cells was showed after the stimulation of vehicle or anti-IL-1β. (D) BMDMs cells were given with the supernatant of Hepa1-6-SLC7A11 with the stimulation of vehicle, anti-IL-1β, vehicle (PBS) or anakinra. The migrative ability of BMDMs cells was showed. (E) HFHC treated-NASH mice with SLC7A11 downregulation were treated with vehicle, anti-IL-1β, vehicle (PBS) or anakinra. HE, Oil Red O, Masson, Sirius Red, and α-SMA staining were demonstrated in these groups of mice. (F) Representative IF staining showed Ly6G and F4/80 in these groups of mice. (G) Graphs showed the serum ALT and AST in mice (n = 6/group). (For interpretation of the references to colour in this figure legend, the reader is referred to the Web version of this article.)

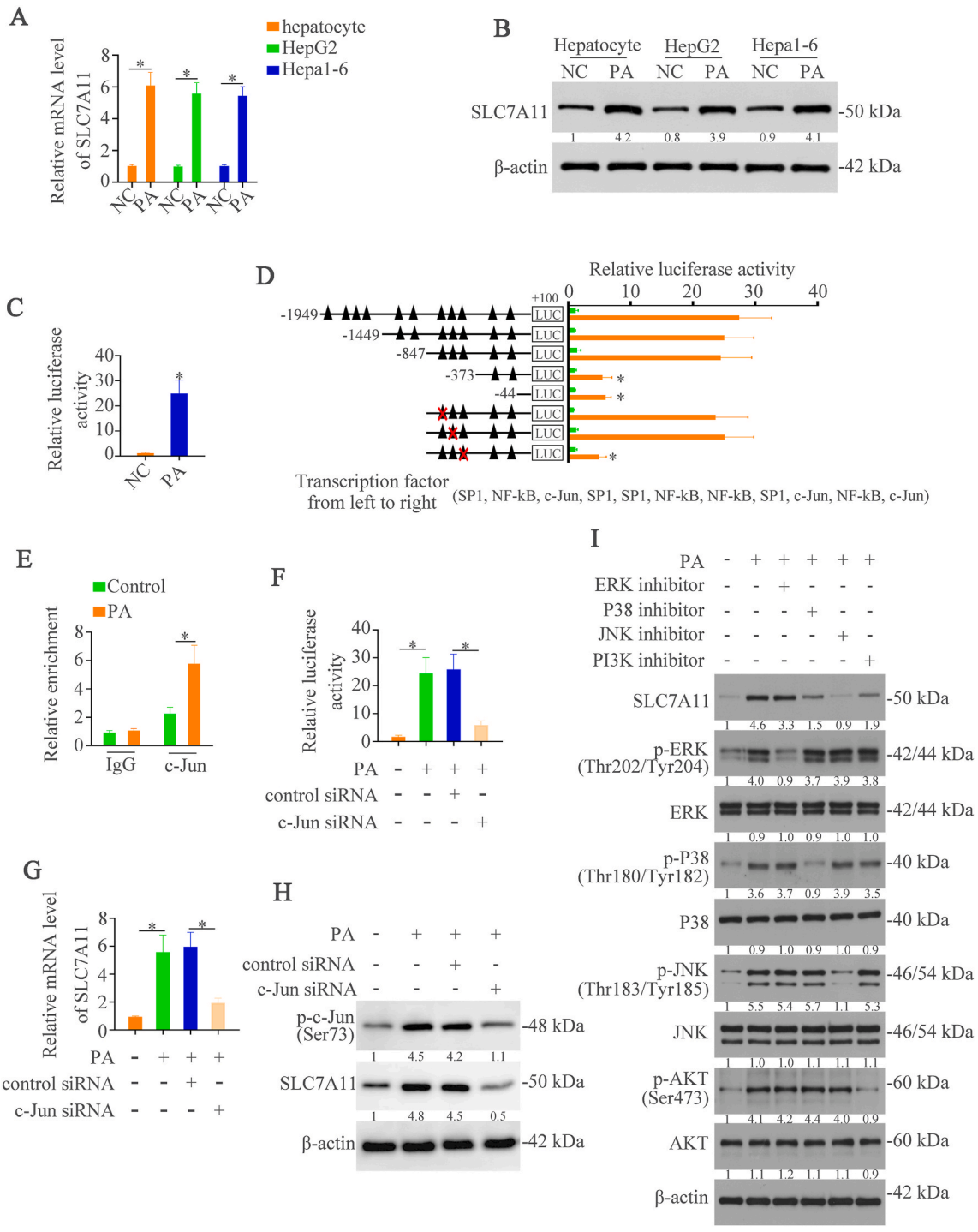

Fig. 8. Lipid-induced JNK-c-Jun pathway contributes to the upregulation of SLC7A11 in NASH
(A) The mRNA expression of *SLC7A11* in the hepatocyte, HepG2 and Hepa1-6 cells with or without PA treatment. (B) The protein level of SLC7A11 in the hepatocyte, HepG2 and Hepa1-6 cells with or without PA treatment. (C) Luciferase activity of SLC7A11 mRNA promoter was detected in the Hepa1-6 cells with or without PA treatment. (D) Truncated and mutated *SLC7A11* promoter sequences were established and transfected in Hepa1-6 cells under PA treatment. Luciferase activity was detected. (E) Ch-IP analysis was used to detected the binding of c-Jun and *SLC7A11* promoter in the Hepa1-6 cells with or without PA treatment. (F) Luciferase activity of *SLC7A11* mRNA promoter was detected in the Hepa1-6 cells transfected with control siRNA or c-Jun siRNA under the PA treatment. (G) The mRNA expression of SLC7A11 in indicated cells. (H) Western blot demonstrated the expression of p-c-Jun (Ser73) and SLC7A11 in indicated cells. (I) ERK, p38, JNK, or PI3K pathway inhibitors were applied in Hepa1-6 cells under PA treatment. Expression of SLC7A11, total and phosphorylated ERK, JNK, p38, and AKT was detected by western blot.

4. Discussion

NASH is considered the progressive form of NAFLD and is characterized by liver steatosis, inflammation, hepatocellular injury and different degrees of fibrosis [2]. Almost one-third of patients with NASH might progress to advanced fibrosis or cirrhosis, which translates to increased liver-related mortality owing to complications of cirrhosis, including HCC [2]. Although several mechanisms underlie NASH

development and progression, the identification of those factors that trigger inflammation, thereby fueling the transition from NAFLD to NASH is still urgent. In this study, we found that SLC7A11 was upregulated in clinical NASH tissues and NASH mice models. Knockdown or knockout of SLC7A11 expression aggravated hepatic lipid accumulation, inflammation, fibrosis and recruited macrophages and neutrophils. However, the upregulation of SLC7A11 had the reverse effect. These results indicated that SLC7A11 played a protective role in NASH. Mechanically, SLC7A11 decreased ROS level through importing cystine and activated AMPK pathway. Ros block by NAC could activate the AMPK pathway. Meanwhile, SLC7A11 decreased αKG content and inhibited PHD activity, which promoted AMPK activation. DM-αKG suppressed AMPK activation induced by SLC7A11 under PA treatment. The AMPK inhibitor compound C (CC) or DM-αKG treatment worsen hepatic lipid accumulation, inflammation, fibrosis and increased recruitment of macrophages and neutrophils in *vivo*. SLC7A11 also triggered inflammasomes inactivation by AMPK activation-induced mitophagy. IL-1β released from NLRP3 inflammasome promoted liver fibrosis and recruited myeloid cells, which contributed to SLC7A11 knockdown-induced NASH progression. Furthermore, inhibition of IL-1β by anti-IL-1β or Anakinra could decrease hepatic inflammation, fibrosis and liver injury. Finally, we found that lipid could upregulate SLC7A11 expression. Luciferase reporter and Chip assays identified the transcription factor c-jun that activated by lipid-induced JNK pathway contributed to the upregulation of SLC7A11. These works indicated the important role of SLC7A11 in decreasing inflammation and impairing NASH progression.

AMPK is a heterotrimeric protein kinase complex, which senses energy statue and can be activated by low energy status [51,52]. Inactivation of AMPK is occurred in during obesity and hyperglycemia [30]. Therefore, AMPK activation has become an attractive potential candidate for the treatment of metabolic diseases including NAFLD [32]. In this research, we demonstrated that SLC7A11 could activate AMPK and thus decrease NASH progression. SLC7A11 outport cysteine and increased GSH level, which decreased ROS level. ROS has been reported to activate or inactivate AMPK, which could be a process that is context-dependent [53]. The reason for this might be due to different cell models, methodological or biological differences, and different methodologies in measuring ROS level. In our study, we found that SLC7A11-induced decrease of ROS inactivated AMPK at Thr172 phosphorylation. Meanwhile, we found that SLC7A11 could decrease αKG level and weaken PHD activity. PHD has been reported to inhibit NF-kB through blocking pIKK activity [24]. However, whether it could regulate AMPK activation is unclear. In this study, we also illustrated that SLC7A11 activated AMPK by inhibiting αKG/PHD activity. Therefore, SLC7A11 upregulation could impair NASH progression by activating AMPK.

Inflammasomes are cytoplasmic multi-protein complexes including one of several NLR and PYHIN proteins, including NLRP1, NLRP3, NLRC4, and AIM2 [54]. Studies have found the important role of inflammasomes in NAFLD and NASH. A research article has found that NLRP6 and NLRP3 inflammasomes and the effector protein IL-18 exacerbated hepatic steatosis and inflammation via modulation of the gut microbiota [55]. However, some articles also found that inflammasomes could induce liver inflammation, liver fibrosis and NASH progression [42,43]. Researches have demonstrated that AMPK could regulate inflammasomes activation by mitophagy-induced clear of damaged mitochondria, which could induce NLRP3 activation [56,57]. In this study, we found that SLC7A11 inactivated NLRP3 inflammasome through AMPK-induced mitophagy.

In summary, in this study, we found a new role of SLC7A11 in NASH progression by regulating oxidative and mitochondrial metabolism, which might be a potential target.

CRediT authorship contribution statement

Tingting Lv: Data curation. **Xiude Fan:** Data curation. **Chang He:** Data curation. **Suwei Zhu:** Methodology. **Xiaofeng Xiong:** Methodology. **Wei Yan:** Investigation. **Mei Liu:** Investigation. **Hongwei Xu:** Supervision. **Ruihua Shi:** Supervision. **Qin He:** Writing – review & editing, Writing – original draft, Supervision, Funding acquisition.

Declaration of competing interest

The authors declare that they have no competing interests.

Data availability

Data will be made available on request.

Acknowledgement

This work was supported by National Natural Science Foundation of China (82203654, 82300810), Natural Science Foundation of Shandong Province (ZR2022QH070, ZR2022QH349) and Clinical Science and Technology Innovation Program of Jinan (202134039). We thank the figdraw (www.figdraw.com) for graphical abstract.

Appendix A. Supplementary data

Supplementary data to this article can be found online at https://doi.org/10.1016/j.redox.2024.103159.

References

[1] A. Geier, D. Tiniakos, H. Denk, M. Trauner, From the origin of NASH to the future of metabolic fatty liver disease, Gut 70 (2021) 1570–1579.
[2] M.E. Rinella, Nonalcoholic fatty liver disease: a systematic review, JAMA 313 (2015) 2263–2273.
[3] Z.M. Younossi, A.B. Koenig, D. Abdelatif, Y. Fazel, L. Henry, M. Wymer, Global epidemiology of nonalcoholic fatty liver disease-Meta-analytic assessment of prevalence, incidence, and outcomes, Hepatology 64 (2016) 73–84.
[4] R. Vuppalanchi, M. Noureddin, N. Alkhouri, A.J. Sanyal, Therapeutic pipeline in nonalcoholic steatohepatitis, Nat. Rev. Gastroenterol. Hepatol. 18 (2021) 373–392.
[5] T. Huby, E.L. Gautier, Immune cell-mediated features of non-alcoholic steatohepatitis, Nat. Rev. Immunol. 22 (2022) 429–443.
[6] L. Ding, W. Sun, M. Balaz, A. He, M. Klug, S. Wieland, R. Caiazzo, V. Raverdy, F. Pattou, P. Lefebvre, I.J. Lodhi, B. Staels, M. Heim, C. Wolfrum, Peroxisomal beta-oxidation acts as a sensor for intracellular fatty acids and regulates lipolysis, Nat. Metab. 3 (2021) 1648–1661.
[7] D.H. Lee, J.S. Park, Y.S. Lee, S.H. Bae, PERK prevents hepatic lipotoxicity by activating the p62-ULK1 axis-mediated noncanonical KEAP1-Nrf2 pathway, Redox Biol. 50 (2022) 102235.
[8] Z. Chen, R. Tian, Z. She, J. Cai, H. Li, Role of oxidative stress in the pathogenesis of nonalcoholic fatty liver disease, Free Radic. Biol. Med. 152 (2020) 116–141.
[9] H. Gao, Z. Jin, G. Bandyopadhyay, G. Wang, D. Zhang, K.C.E. Rocha, X. Liu, H. Zhao, T. Kisseleva, D.A. Brenner, M. Karin, W. Ying, Aberrant iron distribution via hepatocyte-stellate cell axis drives liver lipogenesis and fibrosis, Cell Metabol. 34 (2022) 1201–1213 e1205.
[10] Q. Zhao, J. Liu, H. Deng, R. Ma, J.Y. Liao, H. Liang, J. Hu, J. Li, Z. Guo, J. Cai, X. Xu, Z. Gao, S. Su, Targeting mitochondria-located circRNA SCAR alleviates NASH via reducing mROS output, Cell 183 (2020) 76–93 e22.
[11] E. Piccinin, G. Villani, A. Moschetta, Metabolic aspects in NAFLD, NASH and hepatocellular carcinoma: the role of PGC1 coactivators, Nat. Rev. Gastroenterol. Hepatol. 16 (2019) 160–174.
[12] V.T. Samuel, G.I. Shulman, Nonalcoholic fatty liver disease as a nexus of metabolic and hepatic diseases, Cell Metabol. 27 (2018) 22–41.
[13] S. Maschalidi, P. Mehrotra, B.N. Keceli, H.K.L. De Cleene, K. Lecomte, R. Van der Cruyssen, P. Janssen, J. Pinney, G. van Loo, D. Elewaut, A. Massie, E. Hoste, K. S. Ravichandran, Targeting SLC7A11 improves efferocytosis by dendritic cells and wound healing in diabetes, Nature 606 (2022) 776–784.
[14] K.K. Saini, P. Chaturvedi, A. Sinha, M.P. Singh, M.A. Khan, A. Verma, M. A. Nengroo, S.R. Satrusal, S. Meena, A. Singh, S. Srivastava, J. Sarkar, D. Datta, Loss of PERK function promotes ferroptosis by downregulating SLC7A11 (System Xc(-)) in colorectal cancer, Redox Biol. 65 (2023) 102833.
[15] Q. He, M. Liu, W. Huang, X. Chen, B. Zhang, T. Zhang, Y. Wang, D. Liu, M. Xie, X. Ji, M. Sun, D. Tian, L. Xia, IL-1beta-Induced elevation of solute carrier family 7 member 11 promotes hepatocellular carcinoma metastasis through up-regulating programmed death ligand 1 and colony-stimulating factor 1, Hepatology 74 (2021) 3174–3193.

[16] S. Sutti, E. Albano, Adaptive immunity: an emerging player in the progression of NAFLD, Nat. Rev. Gastroenterol. Hepatol. 17 (2020) 81–92.
[17] Y. Rotman, A.J. Sanyal, Current and upcoming pharmacotherapy for non-alcoholic fatty liver disease, Gut 66 (2017) 180–190.
[18] X. Yang, D. Sun, H. Xiang, S. Wang, Y. Huang, L. Li, X. Cheng, H. Liu, F. Hu, Y. Cheng, T. Ma, M. Hu, H. Tian, S. Tian, Y. Zhou, P. Zhang, X.J. Zhang, Y.X. Ji, Y. Hu, H. Li, Z.G. She, Hepatocyte SH3RF2 deficiency is a key aggravator for NAFLD, Hepatology 74 (2021) 1319–1338.
[19] Z. Zhang, X. Xu, W. Tian, R. Jiang, Y. Lu, Q. Sun, R. Fu, Q. He, J. Wang, Y. Liu, H. Yu, B. Sun, ARRB1 inhibits non-alcoholic steatohepatitis progression by promoting GDF15 maturation, J. Hepatol. 72 (2020) 976–989.
[20] P.X. Wang, Y.X. Ji, X.J. Zhang, L.P. Zhao, Z.Z. Yan, P. Zhang, L.J. Shen, X. Yang, J. Fang, S. Tian, X.Y. Zhu, J. Gong, X. Zhang, Q.F. Wei, Y. Wang, J. Li, L. Wan, Q. Xie, Z.G. She, Z. Wang, Z. Huang, H. Li, Targeting CASP8 and FADD-like apoptosis regulator ameliorates nonalcoholic steatohepatitis in mice and nonhuman primates, Nat. Med. 23 (2017) 439–449.
[21] B. Liu, L. Xiang, J. Ji, W. Liu, Y. Chen, M. Xia, Y. Liu, W. Liu, P. Zhu, Y. Jin, Y. Han, J. Lu, X. Li, M. Zheng, Y. Lu, Sparcl1 promotes nonalcoholic steatohepatitis progression in mice through upregulation of CCL2, J. Clin. Invest. 131 (2021).
[22] B. Xu, M. Jiang, Y. Chu, W. Wang, D. Chen, X. Li, Z. Zhang, D. Zhang, D. Fan, Y. Nie, F. Shao, K. Wu, J. Liang, Gasdermin D plays a key role as a pyroptosis executor of non-alcoholic steatohepatitis in humans and mice, J. Hepatol. 68 (2018) 773–782.
[23] T. Lan, Y. Yu, J. Zhang, H. Li, Q. Weng, S. Jiang, S. Tian, T. Xu, S. Hu, G. Yang, Y. Zhang, W. Wang, L. Wang, Q. Zhu, X. Rong, J. Guo, Cordycepin ameliorates nonalcoholic steatohepatitis by activation of the AMP-activated protein kinase signaling pathway, Hepatology 74 (2021) 686–703.
[24] P.S. Liu, H. Wang, X. Li, T. Chao, T. Teav, S. Christen, G. Di Conza, W.C. Cheng, C. H. Chou, M. Vavakova, C. Muret, K. Debackere, M. Mazzone, H.D. Huang, S. M. Fendt, J. Ivanisevic, P.C. Ho, alpha-ketoglutarate orchestrates macrophage activation through metabolic and epigenetic reprogramming, Nat. Immunol. 18 (2017) 985–994.
[25] I. Kaplanov, Y. Carmi, R. Kornetsky, A. Shemesh, G.V. Shurin, M.R. Shurin, C. A. Dinarello, E. Voronov, R.N. Apte, Blocking IL-1beta reverses the immunosuppression in mouse breast cancer and synergizes with anti-PD-1 for tumor abrogation, Proc. Natl. Acad. Sci. U. S. A. 116 (2019) 1361–1369.
[26] X. Hou, S. Yin, R. Ren, S. Liu, L. Yong, Y. Liu, Y. Li, M.H. Zheng, G. Kunos, B. Gao, H. Wang, Myeloid-cell-specific IL-6 signaling promotes MicroRNA-223-enriched exosome production to attenuate NAFLD-associated fibrosis, Hepatology 74 (2021) 116–132.
[27] H. Wang, W. Mehal, L.E. Nagy, Y. Rotman, Immunological mechanisms and therapeutic targets of fatty liver diseases, Cell. Mol. Immunol. 18 (2021) 73–91.
[28] S. Zhong, L. Li, Y.L. Zhang, L. Zhang, J. Lu, S. Guo, N. Liang, J. Ge, M. Zhu, Y. Tao, Y.C. Wu, H. Yin, Acetaldehyde dehydrogenase 2 interactions with LDLR and AMPK regulate foam cell formation, J. Clin. Invest. 129 (2019) 252–267.
[29] P. Sekar, G. Hsiao, S.H. Hsu, D.Y. Huang, W.W. Lin, C.M. Chan, Metformin inhibits methylglyoxal-induced retinal pigment epithelial cell death and retinopathy via AMPK-dependent mechanisms: reversing mitochondrial dysfunction and upregulating glyoxalase 1, Redox Biol. 64 (2023) 102786.
[30] P. Zhao, X. Sun, C. Chaggan, Z. Liao, K. In Wong, F. He, S. Singh, R. Loomba, M. Karin, J.L. Witztum, A.R. Saltiel, An AMPK-caspase-6 axis controls liver damage in nonalcoholic steatohepatitis, Science 367 (2020) 652–660.
[31] G.R. Steinberg, D.G. Hardie, New insights into activation and function of the AMPK, Nat. Rev. Mol. Cell Biol. (2022).
[32] D. Garcia, K. Hellberg, A. Chaix, M. Wallace, S. Herzig, M.G. Badur, T. Lin, M. N. Shokhirev, A.F.M. Pinto, D.S. Ross, A. Saghatelian, S. Panda, L.E. Dow, C. M. Metallo, R.J. Shaw, Genetic liver-specific AMPK activation protects against diet-induced obesity and NAFLD, Cell Rep. 26 (2019) 192–208 e196.
[33] X. Chen, J. Li, R. Kang, D.J. Klionsky, D. Tang, Ferroptosis: machinery and regulation, Autophagy 17 (2021) 2054–2081.
[34] B. Niu, K. Liao, Y. Zhou, T. Wen, G. Quan, X. Pan, C. Wu, Application of glutathione depletion in cancer therapy: enhanced ROS-based therapy, ferroptosis, and chemotherapy, Biomaterials 277 (2021) 121110.
[35] Y. Zhao, X. Hu, Y. Liu, S. Dong, Z. Wen, W. He, S. Zhang, Q. Huang, M. Shi, ROS signaling under metabolic stress: cross-talk between AMPK and AKT pathway, Mol. Cancer 16 (2017) 79.
[36] W. Liu, Y. Zhao, G. Wang, S. Feng, X. Ge, W. Ye, Z. Wang, Y. Zhu, W. Cai, J. Bai, X. Zhou, TRIM22 inhibits osteosarcoma progression through destabilizing NRF2 and thus activation of ROS/AMPK/mTOR/autophagy signaling, Redox Biol. 53 (2022) 102344.
[37] M. Bauza-Thorbrugge, E. Peris, S. Zamani, P. Micallef, A. Paul, S. Bartesaghi, A. Benrick, I. Wernstedt Asterholm, NRF2 is essential for adaptative browning of white adipocytes, Redox Biol. 68 (2023) 102951.
[38] F. Niu, Z. Li, Y. Ren, Z. Li, H. Guan, Y. Li, Y. Zhang, Y. Li, J. Yang, L. Qian, W. Shi, X. Fan, J. Li, L. Shi, Y. Yu, Y. Xiong, Aberrant hyper-expression of the RNA binding protein GIGYF2 in endothelial cells modulates vascular aging and function, Redox Biol. 65 (2023) 102824.
[39] P. Fraisl, J. Aragones, P. Carmeliet, Inhibition of oxygen sensors as a therapeutic strategy for ischaemic and inflammatory disease, Nat. Rev. Drug Discov. 8 (2009) 139–152.
[40] M.S.J. Mangan, E.J. Olhava, W.R. Roush, H.M. Seidel, G.D. Glick, E. Latz, Targeting the NLRP3 inflammasome in inflammatory diseases, Nat. Rev. Drug Discov. 17 (2018) 588–606.
[41] L. Wang, A.V. Hauenstein, The NLRP3 inflammasome: mechanism of action, role in disease and therapies, Mol. Aspect. Med. 76 (2020) 100889.
[42] A.R. Mridha, A. Wree, A.A.B. Robertson, M.M. Yeh, C.D. Johnson, D.M. Van Rooyen, F. Haczeyni, N.C. Teoh, C. Savard, G.N. Ioannou, S.L. Masters, K. Schroder, M.A. Cooper, A.E. Feldstein, G.C. Farrell, NLRP3 inflammasome blockade reduces liver inflammation and fibrosis in experimental NASH in mice, J. Hepatol. 66 (2017) 1037–1046.
[43] S. Gaul, A. Leszczynska, F. Alegre, B. Kaufmann, C.D. Johnson, L.A. Adams, A. Wree, G. Damm, D. Seehofer, C.J. Calvente, D. Povero, T. Kisseleva, A. Eguchi, M.D. McGeough, H.M. Hoffman, P. Pelegrin, U. Laufs, A.E. Feldstein, Hepatocyte pyroptosis and release of inflammasome particles induce stellate cell activation and liver fibrosis, J. Hepatol. 74 (2021) 156–167.
[44] D.F. Egan, D.B. Shackelford, M.M. Mihaylova, S. Gelino, R.A. Kohnz, W. Mair, D. S. Vasquez, A. Joshi, D.M. Gwinn, R. Taylor, J.M. Asara, J. Fitzpatrick, A. Dillin, B. Viollet, M. Kundu, M. Hansen, R.J. Shaw, Phosphorylation of ULK1 (hATG1) by AMP-activated protein kinase connects energy sensing to mitophagy, Science 331 (2011) 456–461.
[45] E.Q. Toyama, S. Herzig, J. Courchet, T.L. Lewis Jr., O.C. Loson, K. Hellberg, N. P. Young, H. Chen, F. Polleux, D.C. Chan, R.J. Shaw, Metabolism. AMP-activated protein kinase mediates mitochondrial fission in response to energy stress, Science 351 (2016) 275–281.
[46] D. Narendra, A. Tanaka, D.F. Suen, R.J. Youle, Parkin is recruited selectively to impaired mitochondria and promotes their autophagy, J. Cell Biol. 183 (2008) 795–803.
[47] K.K.L. Wu, K. Long, H. Lin, P.M.F. Siu, R.L.C. Hoo, D. Ye, A. Xu, K.K.Y. Cheng, The APPL1-Rab5 axis restricts NLRP3 inflammasome activation through early endosomal-dependent mitophagy in macrophages, Nat. Commun. 12 (2021) 6637.
[48] R. Zhou, A.S. Yazdi, P. Menu, J. Tschopp, A role for mitochondria in NLRP3 inflammasome activation, Nature 469 (2011) 221–225.
[49] S. Schuster, D. Cabrera, M. Arrese, A.E. Feldstein, Triggering and resolution of inflammation in NASH, Nat. Rev. Gastroenterol. Hepatol. 15 (2018) 349–364.
[50] X. Zhang, L. Fan, J. Wu, H. Xu, W.Y. Leung, K. Fu, J. Wu, K. Liu, K. Man, X. Yang, J. Han, J. Ren, J. Yu, Macrophage p38alpha promotes nutritional steatohepatitis through M1 polarization, J. Hepatol. 71 (2019) 163–174.
[51] D.G. Hardie, F.A. Ross, S.A. Hawley, AMPK: a nutrient and energy sensor that maintains energy homeostasis, Nat. Rev. Mol. Cell Biol. 13 (2012) 251–262.
[52] D. Garcia, R.J. Shaw, AMPK: mechanisms of cellular energy sensing and restoration of metabolic balance, Mol. Cell 66 (2017) 789–800.
[53] Y. Ren, H.M. Shen, Critical role of AMPK in redox regulation under glucose starvation, Redox Biol. 25 (2019) 101154.
[54] M. de Carvalho Ribeiro, G. Szabo, Role of the inflammasome in liver disease, Annu. Rev. Pathol. 17 (2022) 345–365.
[55] J. Henao-Mejia, E. Elinav, C. Jin, L. Hao, W.Z. Mehal, T. Strowig, C.A. Thaiss, A. L. Kau, S.C. Eisenbarth, M.J. Jurczak, J.P. Camporez, G.I. Shulman, J.I. Gordon, H. M. Hoffman, R.A. Flavell, Inflammasome-mediated dysbiosis regulates progression of NAFLD and obesity, Nature 482 (2012) 179–185.
[56] D. Bai, J. Du, X. Bu, W. Cao, T. Sun, J. Zhao, Y. Zhao, N. Lu, ALDOA maintains NLRP3 inflammasome activation by controlling AMPK activation, Autophagy 18 (2022) 1673–1693.
[57] E.S. Jung, K. Suh, J. Han, H. Kim, H.S. Kang, W.S. Choi, I. Mook-Jung, Amyloid-beta activates NLRP3 inflammasomes by affecting microglial immunometabolism through the Syk-AMPK pathway, Aging Cell 21 (2022) e13623.